Effects of Signal Quantisation and Spatial Sampling in Reconstructing Surface Density Profiles

Steven Homolya
School of Physics and Materials Engineering
Monash University, Australia
Steven.Homolya@spme.monash.edu.au

Charles F. Osborne
School of Physics and Materials Engineering
Monash University, Australia
Charles.Osborne@spme.monash.edu.au

Imants D. Svalbe
School of Physics and Materials Engineering
Monash University, Australia
Imants.Svalbe@spme.monash.edu.au

Abstract

The density profile of a vibrating surface can be estimated from interferometric observation of the surface modes. This paper evaluates the effects of digital quantisation, in both intensity and space, on the precision of the reconstructed surface density profile, found using the digital samples of an interferogram. The surface determination is shown to be more robust, for a given number of modes, if the observed intensities are smoothed, at the expense of losing fine density variations.

1. Introduction

We consider vibrations of a surface, whose mass surface density is inhomogeneous in space. We demonstrate that the surface density of the object may be determined indirectly by experimental observation of its vibrational modes. Section 2 provides the mathematical definition of the physical system. Section 3 describes an experiment aimed at observing the object in vibration using an interferometer equipped with a photo-detector array, which is interfaced with a computer. A method for estimating the surface density of the object from the experimental data is outlined in section 4. Method for computing error estimates due to signal level quantisation are discussed. Simulated results for a membrane surface are provided in section 5. The use of filtering aimed at reducing the effects of signal quantisation noise is also discussed. In section 6 the key results presented in the paper are summarised.

2. Vibrations of an Inhomogeneous Surface

Transverse linear vibrations of a surface object S are described by an equation of the form

$$Ku = -\omega^2 \sigma u \quad \text{on } S, \tag{1}$$

where K is a linear stiffness operator, such that Ku is the transverse force per unit surface area due to surface deformation specified by transverse displacement $u(x, y) : S \to \mathbb{R}$; σ is the mass surface density or mass per unit surface area; and ω is the frequency of vibration. Solutions u, ω of equation (1) are referred to as natural modes and frequencies of the system respectively. Physical systems described by an equation of the form given in (1) include membranes, plates and curved surfaces or shells [1].

Our proposed method for indirect measurement of the unknown density of a surface object is based on the fact that equation (1) can be rearranged to express the surface density σ in terms of operator *K*, modeshape *u* and frequency ω:

$$\sigma = -\frac{Ku}{\omega^2 u}, \quad \text{when } u \neq 0. \tag{2}$$

Hence if *K* is known, the density of the surface can be determined from one or more vibrational modes and frequencies. The purpose of the work presented here is to demonstrate how this might be done in practice, from u and ω that are found experimentally using holographic interferometry. Specific results are presented in this paper for a membrane with $K = \nabla^2$, however the method is applicable to any surface whose motion is governed by an equation of the form (1).

3. Experimental Observation of Modeshapes

Holographic interferometry has proven to be a powerful tool over the past four decades for studying vibrations of

solid objects [4-8]. Figure 1 shows a schematic depicting a possible experimental setup. Light from a monochromatic source (SRC) is split (BS_1) in space into two components, one of which, the reference wave, is directed towards the observation plane by suitable optics (M $\rightarrow$ BS_2). The other, which passes through BS_1, is used illuminate the vibrating surface at *S*. The light scattered by the surface is collected and directed towards beam splitter BS_2, where it is recombined with the reference wave to produce an interference pattern at the detector D. The detector is interfaced with a computer for displaying and storing the interferograms as greyscale images. A variable phase shifter PS (for example a rotatable glass slide) placed in the path of the reference beam can be employed to change the phase of the wave before it is recombined with waves scattered from S.

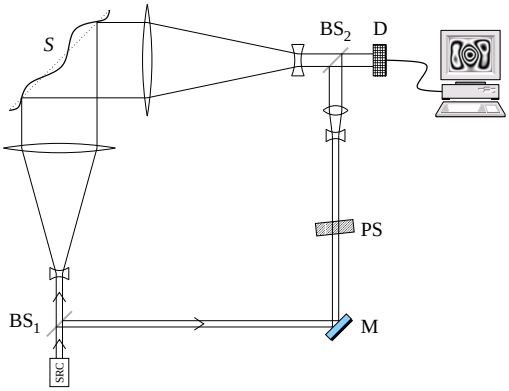

Figure 1. Schematic diagram depicting an experimental setup with an interferometer used to observe vibrations of a surface object S.

A technique suited to digital image processing employs stroboscopic illumination [6-8]. The surface is excited by harmonic forcing at resonance, and made to vibrate in a pure mode u. The strobe is synchronised to the excitation mechanism, so that one pulsed illumination per cycle of oscillation is produced, illuminating the surface at the same phase in each cycle. The interference pattern at the detector corresponds to one due to a static displacement proportional to the vibration amplitude $u(x, y)$. For planar surface S and monochromatic illumination, the intensity at the detector is, within an additive constant,

$$I(x', y') \propto 1 + \cos[2a\pi\, u(x, y) - \phi], \qquad (3)$$

where *a* is the number of fringes per unit increment in displacement u (a constant determined by specifics of the experimental setup [5]), and ϕ is a constant phase term, assuming proper alignment of the apparatus [2, p.112]. The value of ϕ may be altered at the phase shifter PS (Figure 1). For each vibrational mode u, at least two interferograms are needed in order to determine the phase $\varphi = 2\pi a u$ of the wave at the detector. Let us assume that two intensities are recorded, one with $\phi = 0$ and another with $\phi = \pi/2$:

$$I_1'(x', y') \propto I_1(x, y) = \frac{1}{2}(1 + \cos\varphi), \qquad (4)$$

$$I_2'(x', y') \propto I_2(x, y) = \frac{1}{2}(1 + \sin\varphi). \qquad (5)$$

Assuming that the output of the detector array is calibrated to give high contrast in the recorded images, and that the detector samples the light intensity at sites of a $L \times W$ square lattice in the observation plane, the results of the experiment are two $L \times W$ greyscale images G_1 and G_2 corresponding to intensities I_1 and I_2 respectively:

$$G_j(p, q) = \mathrm{round}\,[(D + \Delta)\, I_j(ph, qh) + \delta]\,, \qquad (6)$$

where $j = 1, 2$; p and q are integers in $[1, L]$ and $[1, W]$ respectively; $D + 1$ is the number of shades of greys in the image; h is the sampling interval at S; Δ and δ are errors in calibrating the detector output; and 'round' is a function which gives the integer closest to its argument. Ideally two further arrays, δG_1 and δG_2, would be used to specify the combined effect of experimental and quantisation errors, in G_1 and G_2 respectively, such that

$$D\, I_j(ph, qh) = G_j(p, q) \pm \delta G_j(p, q). \qquad (7)$$

Expressing the sampled phase, $\varphi(ph, qh) \bmod 2\pi \simeq \varphi_{pq}$, corresponding to sampled intensities $I_j(ph, qh)$ of (4,5), in terms of pixel values G_j, and considering relation (7), the errors $\delta\varphi_{pq}$ in the phase, $\varphi(ph, qh) \bmod 2\pi = \varphi_{pq} \pm \delta\varphi_{pq}$, can be estimated by

$$\delta\varphi_{pq} = \min\left(\frac{\delta G_1}{|G_2 - D/2|}, \frac{\delta G_2}{|G_1 - D/2|}\right), \qquad (8)$$

which is correct to first order in the errors δG_j. For the sake of definiteness, we assume in what follows that calibration errors Δ and δ are at most half one greylevel, and that the errors introduced by the quantisation of the signals I_j are much greater than all other experimental errors combined. Then, by allowing for rounding errors in (6) we have $\delta G_j = 0.5 G_j/D + 1$, so we can estimate errors in the phase from greyvalues G_j alone, using equation (8).

Once estimates for the phase $\varphi \bmod 2\pi$ have been deduced from the two interferograms $G_{1,2}$, estimates for the true phase of the wave $\varphi(ph, qh) = 2\pi a u(ph, qh)$ can be can be obtained by unwrapping the mod 2π phase. For results presented in section 5, phase unwrapping was performed using a simple sequential linear scanning algorithm due to Takeda [4, p.204-5]. For the algorithm to work, the sampling density must be sufficiently large so that no fringes are missed (phase changes must be less than π between nearest neighbour pixels), and the data must be free

of excessive noise (speckle, for example). More sophisticated algorithms are available for unwrapping noisy and/or undersampled data [3].

As the unwrapped phase φ_{pq} is proportional to the amplitude of vibration at grid-points $(x, y) = (ph, qh)$, it is also a sampled solution $u_{pq} = \varphi_{pq} \simeq u(ph, qh)$ of equation (1), within known experimental errors $\delta u_{pq} = \delta\varphi_{pq}$. With ω measured as the resonance frequency for displacement amplitude u, a sampled solution (ω, u_{pq}) of equation (1) is obtained by the experiment described above. Examples of simulated interferogram data for $D = 255$ and $L = W = 60$ are shown in Figure 2.

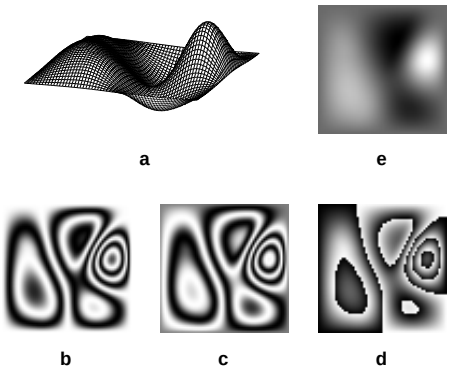

Figure 2. (a) Sixth vibrational mode of a membrane with non-uniform surface density; (b) corresponding cos fringes; (c) sin fringes; (d) wrapped phase; (e) unwrapped phase.

4. Density from Sampled Modeshapes

By approximating the behaviour of the displacement u, at sampling locations $(x, y) = (ph, qh)$, using local polynomial interpolation on the sampled data, the transverse force per unit surface area may be approximated as

$$K\, u(x,y)|_{(x,y)=(ph,qh)} \simeq \sum_{rs} K_{pq,rs}\, u_{rs}, \qquad (9)$$

where for a membrane with surface tension of unity we have

$$K = \nabla^2 = \partial_x^2 + \partial_y^2$$

and

$$K_{pq,rs} = \begin{cases} C_{p-r}/h^2, & \text{if } q = s \text{ and } |p-r| \le N, \\ C_{q-s}/h^2, & \text{if } p = r \text{ and } |q-s| \le N, \\ 0, & \text{otherwise,} \end{cases} \qquad (10)$$

where coefficients C_n only depend on the order $2N$ of the interpolating polynomial. The values of coefficients C_n for interpolation of up to 8^{th} order up are summarised in Table 1.

Table 1. Coefficients used to estimate 2nd order derivatives for various order interpolation schemes as discussed in the text.

N	C_0	C_1	C_2	C_3	C_4
1	-2	1			
2	-5/2	4/3	-1/12		
3	-49/18	3/2	-3/20	1/90	
4	-205/72	8/5	-1/5	8/315	-1/560

Using relation (9), the equation of motion (1) may be approximated by

$$\sum_{rs} K_{pq,rs} u_{rs} = -\omega^2 \sigma_{pq} u_{pq}, \qquad (11)$$

where u_{pq} and σ_{pq} are the sampled values of functions u and σ respectively. The matrix of coefficients $\mathbf{K} = [K_{pq,rs}]$, the stiffness matrix, is the discrete counterpart of the stiffness operator K. From equation (11) we obtain the following expression for the sampled density:

$$\sigma_{pq} = \frac{-\sum_{rs} K_{pq,rs} u_{rs}}{\omega^2 u_{pq}}, \quad u_{pq} \neq 0, \qquad (12)$$

which is a discrete approximation to equation (2).

Let us suppose that a sampled modeshape u_{pq} and the associated natural frequency ω have been deduced experimentally within $\pm\delta u_{pq}$ and $\pm\delta\omega$ errors respectively. Assuming that these errors dominate over those arising from discrete approximation (11) of the equation of motion (1), the errors $\delta\sigma_{pq}$ in the computed values of σ, such that $\sigma(ph, qh) = \sigma_{pq} \pm \delta\sigma_{pq}$, may be estimated from equation (12) as

$$\delta\sigma_{pq} = \left(\frac{\sum_{rs} |K_{pq,rs}|\, \delta u_{rs}}{|\sum_{rs} K_{pq,rs} u_{rs}|} + \frac{\delta u_{pq}}{|u_{pq}|} + 2\frac{\delta\omega}{\omega} \right) \sigma_{pq}, \qquad (13)$$

which is correct to first order in δu_{ij} and $\delta\omega$. When several modes and frequencies are known, equation (12) will provide several corresponding estimates for the surface density. By comparing the error estimates given by (13), we can select the σ_{pq} with the smallest errors to combine the results from all observed modes.

5. Results for Simulated Data

Here we present results of simulations of the surface reconstruction method for two membranes with inhomogeneous surface densities, and a surface tension of unity. The membranes were assumed fixed to a rigid square boundary. The first step in simulating the experimental data involved solution of the equations of motion (1) for the first 20 natural frequencies and modes, by discretisation on a high resolution, 240×240, grid, as discussed in section 4. 8^{th} order polynomial interpolations were used to approximate the

Laplacian. The resulting matrix equations (11) were solved using the Lanczos algorithm [9].

The high resolution modeshape data was down-sampled onto a 60×60 grid to obtain assumed exact values $u(ph, qh)$ of displacement amplitude $u(x, y)$ at grid points $(x, y) = h \times (p, q)$. Corresponding exact intensities $I_{1,2}(x, y)$ in the detector plane of the interferometer were computed using equations (4,5), with constant a adjusted to give similar fringe densities for all modes, keeping fringe spacing greater than two grid spacings in order to ensure reliability of subsequent phase unwrapping. (In an actual experiment this would involve adjusting the amplitude of the applied harmonic force until the desired fringe spacing is attained.) Using relation (6), the two greyscale images $G_{1,2}$ were generated from the computed intensities $I_{1,2}$, with calibration errors Δ and δ chosen at random from the interval $[-0.5, 0.5]$ for each set of modeshapes. D was set to 15, 63 or 255, which correspond to 16-, 64- and 256-greylevel images respectively. The quantised interferograms, and associated error estimates given by (8), where $\delta G_j = 0.5 G_j / D + 1$, were treated as the result of an experiment described in section 3. Thus, approximations u_{pq} to the sampled modes along with error estimates δu_{pq} were obtained from the simulated experimental data. For sake of simplicity, frequencies ω were assumed exact with $\delta\omega = 0$, as this makes no difference to the ensuing discussion. The surface reconstruction method described in section 4 was applied to the simulated experimental data in an attempt to recover the mass surface densities of the membranes. Fourth order interpolations were used in the solution of the inverse problem.

5.1. Test Densities

The two density functions used in the simulations are shown as greyscale plots in Figure 3a and b. The density of system 1, plotted in Figure 3a, comprises of four regions, within each of which its value is a constant equal to 1, 2 or 3 (lighter shades of grey represent larger values). The density changes abruptly at the boundaries between homogeneous regions. The image shown in Figure 3b represents the density of system 2, which is a continuous function of (x, y), and is a superposition of planewaves with randomly generated relative phases, which amounts to bandwidth-limited white-noise. The global extrema for the density function are 0.25 and 2.0. In the Figure 3b black and white correspond to 0 and 2.05 respectively. The reason our two choices of σ considered here is that together they illustrate all key features of the surface reconstruction method.

a b

Figure 3. Greyscale plots of membrane surface density test functions, sampled on a 60×60 grid: (a) composite of four well defined homogeneous regions where densities are equal to 1 (darkest), 2 (medium grey), 3 (lightest); (b) Low-pass filtered white noise.

5.2. Reconstruction from High Depth Resolution Data

Figure 4 shows the densities reconstructed from interferograms of the first five and the first twenty modes of the membranes, with simulated detector depth resolution of 256 intensity levels. Pixels in black represent grid-points where the estimated errors in the computed density is greater than 50%. Both reconstructions show considerable speckle noise and some blurring or loss of contrast. However, these are within estimated errors, which have proved to be conservative, typically less than 20% of the true error, except at internal boundaries shared by $\sigma = 1, 2$ and $\sigma = 1, 3$ constant density regions of system 1. Here, the blurred edges are due to errors introduced by discretisation of the stiffness operator, and are present for all D, as confirmed by simulations with D up to 10^7. For both systems, the density computations show poor accuracy near nodal lines $u = 0$, as would be expected from (13).

Reconstructions from lower depth resolution interferogram images have failed, with no computed density values with error estimates below 50% for 16 greylevel interferograms, and only about 10% of the sampled density array recovered from the first 20 modes of the two membranes with 64 greylevels. Since we are assuming that errors introduced by the quantisation of the light intensity at the detector are much greater than other experimental errors, results of the simulations would imply a requirement for accuracy significantly better than $1 \div 256$ in the experimental data for it to be useful, which is unacceptable. Fortunately, this is not required, and low depth interferograms can be used to obtain good estimates for the surface density, as we shall discuss in the following sections.

a b c d

Figure 4. Reconstructed membrane surface densities computed from 256-greylevel interferograms

of modes 1 to 5 (a,b) and modes 1 to 20 (c,d).

5.3. Down-sampled Low Depth Data

The large error estimates in the density computed from low depth resolution interferograms is due to the inaccuracy of the approximation on the left hand side of (11), involving the stiffness matrix $\mathbf{K}$, to $\nabla^2 u$. Since coefficients $K_{pq,rs}$, given by (10), are proportional to h^{-2}, the error in the reconstructed density, as given by (13), diverges with increasing spatial resolution as h^{-2}. We can compensate for this by increasing the accuracy of the data, which would imply that we need to increase the depth of the interferogram images with $D \sim h^{-2}$. Alternatively, the sampling resolution can be reduced for the low depth data, increasing h as $1/\sqrt{D}$. For the 16-greylevel interferograms obtained in our simulations, this would imply that in order to to attain estimated accuracies in the reconstructed densities similar to those obtained for the 256-greylevel images, the resolution should be reduced from 60×60 to 15×15. Results of simulations for $D = 15$, using reduced resolution phase arrays are shown in Figure 5. The reconstructions compare favourably with corresponding results shown in Figure 4.

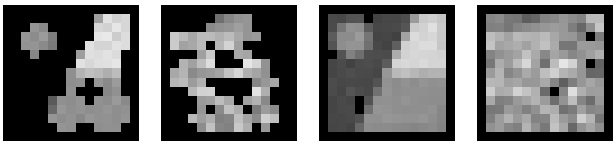

a b c d

Figure 5. Reconstructed membrane surface densities computed from 16-greylevel interferograms of modes 1 to 5 (a,b) and modes 1 to 20 (c,d) with down-sampling used to reduce errors.

5.4. Use of Filters with Low Depth Data

The main drawback of reducing spatial resolution is that it introduces further errors in the discrete approximation (9) of the stiffness operator. This problem can be overcome by appropriate pre-processing of the full resolution unwrapped phase data before applying the transformation (12) to obtain the surface density. This may be achieved by applying a low-pass filter data, letting

$$u_{pq} \to \frac{\sum_{ij} F_{i-p,j-q} u_{ij}}{\sum_{ij} F_{ij}}, \qquad (14)$$

where the sum is over the entire array ($i = 1..L, j = 1..W$), and the Gaussian blur window, defined by coefficients F_{pq}, is given by

$$F_{pq} = e^{-(p^2+q^2)/R^2},$$

where R is the radius of the filter.

If we use the filtered phase to calculate the density from equation (2), we get

$$\sigma_{pq} = \frac{-\sum_{ij,rs} K_{pq,rs} F_{i-r,j-s} u_{ij}}{\omega^2 \sum_{ij} F_{i-p,j-p} u_{ij}},$$

where u_{ij} correspond to the unfiltered data. Relative errors for the densities σ_{pq} computed from the filtered phase may now be estimated, to first order in errors δu_{ij} and $\delta\omega$, as

$$\frac{\delta\sigma_{pq}}{\sigma_{pq}} = \frac{\sum_{ij} |\sum_{rs} K_{pq,rs} F_{i-r,j-s}| \, \delta u_{ij}}{|\sum_{ij,rs} K_{pq,rs} F_{i-r,j-s} u_{ij}|} + \frac{\sum_{ij} |F_{i-r,j-s}| \, \delta u_{ij}}{|\sum_{ij} F_{i-r,j-s} u_{ij}|} + 2\frac{\delta\omega}{\omega}. \qquad (15)$$

Filtering works because in the first term on the right hand side of (15), which is the relative error in Ku, it is the coefficients $K_{pq,rs}$ that are being blurred and not the errors themselves (as is the case for the second term, which will remain similar in magnitude before and after filtering). As $K_{pq,rs}$ alternate in sign with increments in r or s, and the filter gives a weighted average over these, the magnitude of this average is going to be smaller than the sum of the magnitudes of $K_{pq,rs}$ in (13). Hence the error estimates as given by (15) are generally reduced by filtering. We can check whether we have chosen a reasonable value for the filter radius by comparing filtered and unfiltered data. If the former is not within estimated error of the latter, the filter radius needs to be decreased.

While the expression given in (15) can be used to compute the reduced error estimates for σ_{pq}, the computation of the first sum on the right hand side of (15) for each (p, q) is excessively time consuming. However, instead of computing the errors directly, we can estimate the ratio ρ of filtered and raw data errors in Ku by comparing the magnitude of coefficients of δu_{ij} in the corresponding terms of (13) and (15):

$$\rho \simeq \sum_{ij} |\sum_{rs} K_{pq,rs} F_{i-r,j-s}| \, / \sum_{ij} |K_{pq,ij}| \, . \qquad (16)$$

Since the summations involve all (i, j) and (r, s), and $K_{pq,rs}$ only depend on the differences between indeces, $p - r$ and $q - s$, ρ is independent of (p, q). Once ρ is computed, the reduced error estimates for σ_{pq} may be obtained from (13), except that the first term inside the brackets should be multiplied by ρ.

In our experience, the error reduction factor ρ given by (16) is overly conservative, especially when starting with low depth resolution interferograms, which require stronger filtering (larger R). More reasonable error estimates are obtained if we assume the applicability of the central limit theorem to the sum of the actual errors Δu_{ij} in u_{ij}, which gives the error $\Delta(Ku)$ in Ku as $\Delta(Ku) = \sum_{ij} |\sum_{rs} K_{pq,rs} F_{i-r,j-s}| \, \Delta u_{ij}$. Thus

$$\rho \simeq \sqrt{\max_{ij}(|\sum_{rs} K_{pq,rs} F_{i-r,j-s}|)}$$

$$\times \sqrt{\sum_{ij} |\sum_{rs} K_{pq,rs} F_{i-r,j-s}|} \Big/ \sum_{ij} |K_{pq,ij}| \, .$$

Reconstructions computed from low-pass filtered, low depth resolution phase data are shown in Figure 6. Blur filter of radius $R = 2$ was applied to phase arrays computed from 16-greylevel interferograms. On inspection, reconstructions appear to have recovered more detail in the surface densities than those obtained from the reduced resolution phase arrays (Figure 5). However, for system 1 (Figure 6a,c) the results illustrate that suppressing high spatial frequencies in the phase results in a similar reduction in high spatial frequency components of the reconstructed density, seen here as a blurring of boundaries between constant density regions. Reconstructions near the edges of the system (where blur filter windows were symmetrically cropped), are adversely effected, and computed error estimates for densities within one filter radius of the system's boundary are generally not within estimated error of the true values. (Modification of the filter near boundaries was not considered in error calculations, however.) For system 2 (Figure 6b,d), filtering resulted in a loss of contrast in the reconstructed density images.

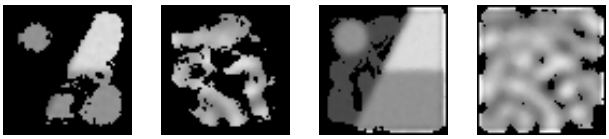

a b c d

Figure 6. Reconstructed membrane surface densities computed from 16-greylevel interferograms of modes 1 to 5 (a,b) and modes 1 to 20 (c,d) with low pass filtering used to reduce errors.

6. Conclusions

We have demonstrated through computer simulations that an interferometer can be used to measure the mass density of a planar surface object by observing interference patterns associated with its vibrational modes. We have analysed errors arising due to finite spatial sampling and signal quantisation in the interferograms, and discussed two strategies for reducing such errors, one involving down-sampling and another spatial filtering. Quantitative analysis of the error reduction methods show good agreement with simulated data for membranes with inhomogeneous densities.

References

[1] Szilard R, "Theory and Analysis of Plates: Classical and Numerical Methods", Prentice-Hall, 1974

[2] Jones R. and Wykes C., "Holographic and Speckle Interferometry: A discussion of the theory, practice and application of the techniques", Cambridge University Press, 1983

[3] Liang Z.-P., *IEEE Trans. Med. Imaging*, "A model based phase unwrapping method"**, 15**, 893-7 (1996)

[4] Robinson D. W. and Reid G. T., "Interferogram Analysis, Digital Fringe Pattern Measurement Techniques", IOP Publishing (1993)

[5] Powell R. L. and Stetson K. A., "Interferometric Vibration Analysis by Wavefront Reconstruction", *Journ. Opt. Soc. Am.* **55** 1593-8 (1965)

[6] Shajenko P. and Johnson C. D., "Stroboscopic Holographic Interferometry", *Applied Physics Letters* **13** 44-6 (1968); Watrasiewicz B. M. and Spicer P., "Vibration Analysis by Stroboscopic Holography", *Nature* **217** 1142-3 (1968); Archbold E. and Ennos A. E., "Observation of Surface Vibration Modes by Stroboscopic Hologram Interferometry", *Nature* **217** 942-3 (1968)

[7] Hariharan P. and Oreb B. F., "Stroboscopic Holographic Interferometry: Application of Digital Techniques", *Optics Communications* **59** 83-6 (1986)

[8] Hariharan P. Oreb B. F. and Freund C. H., "Stroboscopic Holographic Interferometry: Measurements of Vector Components of a Vibration", *Applied Optics* **26** 3899-903 (1987)

[9] Cullum, J. K. and Willoughby R. A., "Lanczos algorithms for large symmetric eigenvalue computations", Boston: Birfhauser (1985)